Supplementary Information

Role of Dy^{3+} ion clusters in CaF_2: Dy^{3+} crystals on yellow and mid–infrared laser characteristics

Longxing Zheng[1,2], Yixiang Huang[1,2], Zhaojie Zhu[1], Yizhi Huang[1], Chaoyang Tu[1], G. Lakshminarayana[3], Yan Wang[1,*]

[1]*State Key Laboratory of Functional Crystals and Devices, Fujian Institute of Research on the Structure of Matter, Chinese Academy of Sciences, Fuzhou 350002, China.*

[2]*University of Chinese Academy of Sciences, Bei Jing City, 100039, P. R. China.*

[3]*Future Technology School, Shenzhen Technology University, Shenzhen 518118, China*

**Corresponding author's E–mail: wy@fjirsm.ac.cn*

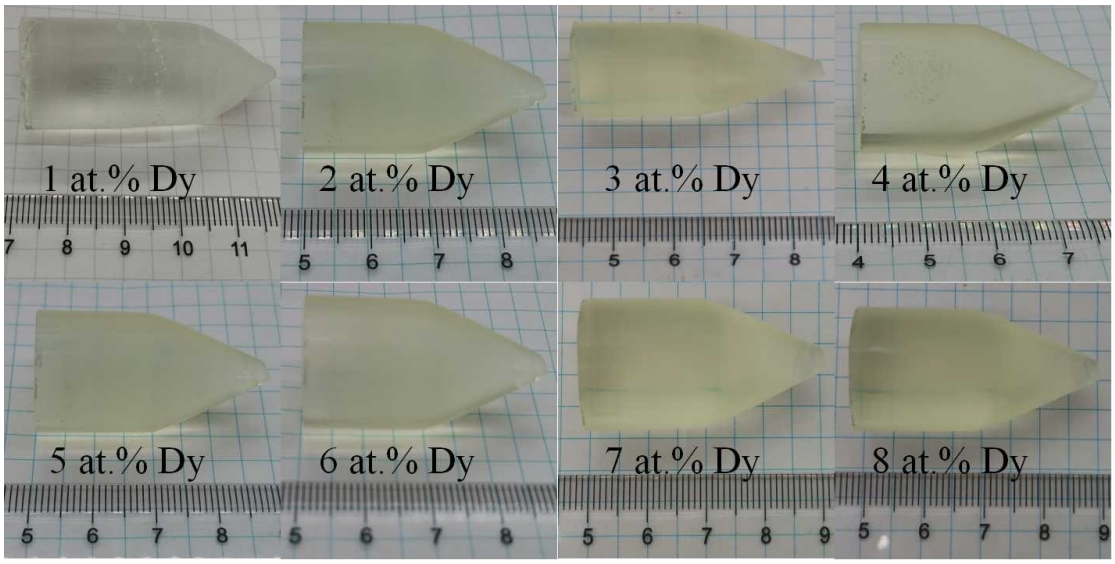

Figure S1. The grown Dy^{3+}: CaF_2 crystals with varying Dy^{3+} doping concentrations.

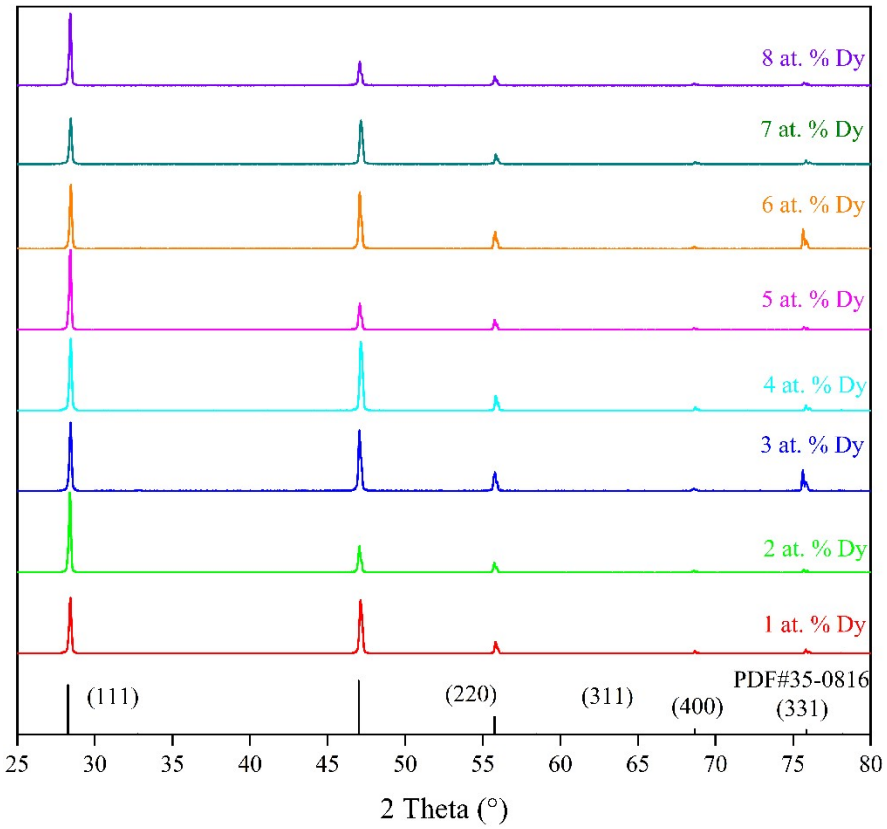

Figure S2. XRD patterns of Dy^{3+}: CaF_2 crystals doped with different concentrations

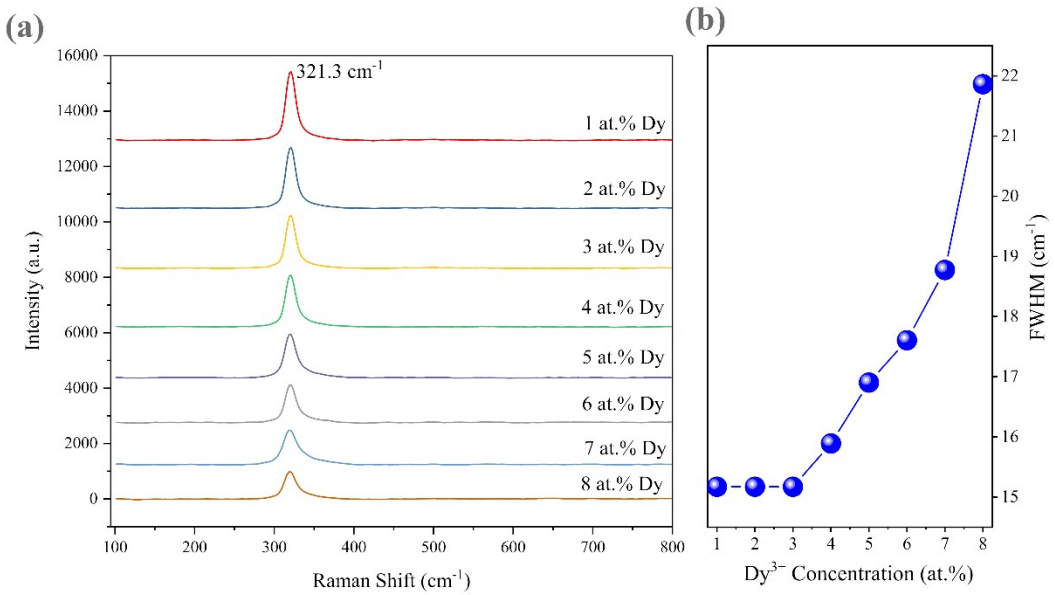

Figure S3. (a) Raman spectra of Dy^{3+}: CaF_2 crystals and (b) FWHM of the Raman peak with different doping concentrations

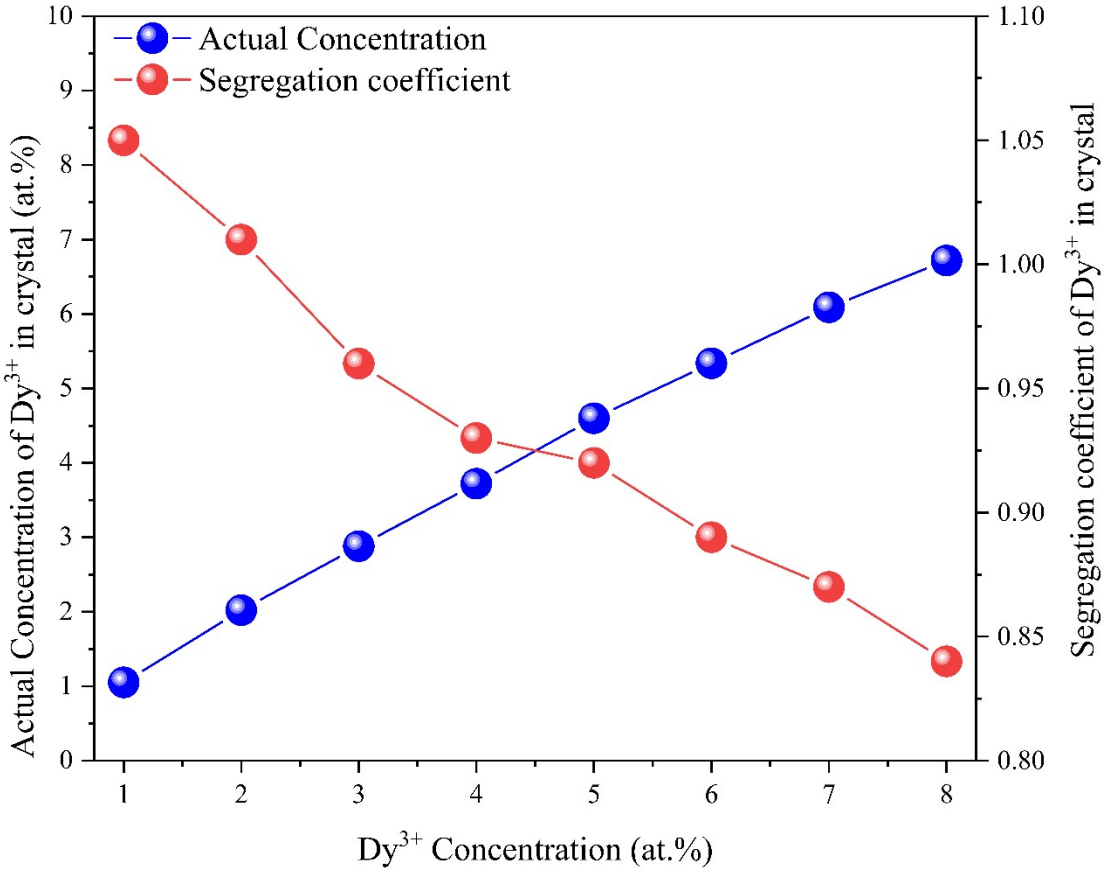

Figure S4. Actual concentration and segregation coefficient of Dy^{3+} in the Dy^{3+}: CaF_2 crystals

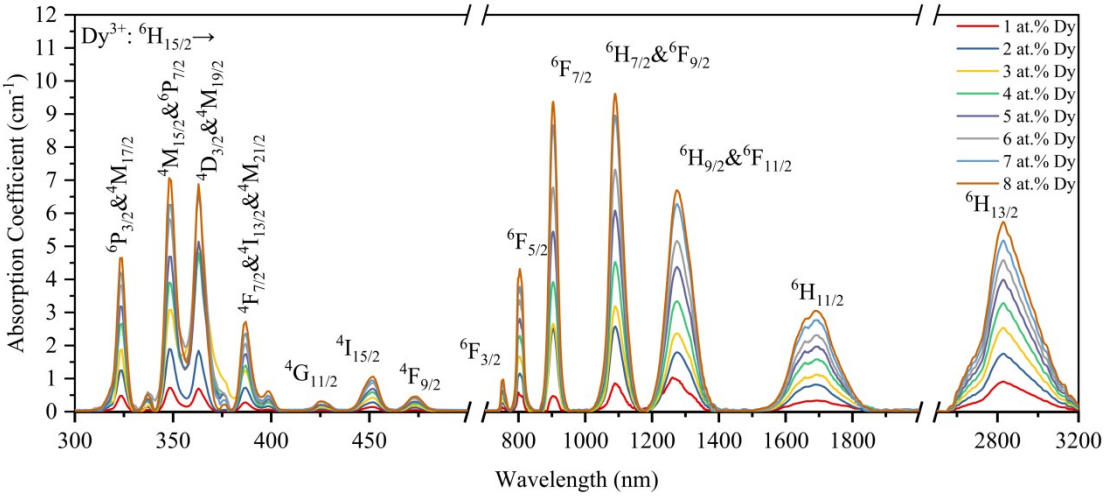

Figure S5. Absorption spectra of Dy^{3+}: CaF_2 crystals with different doping concentrations.

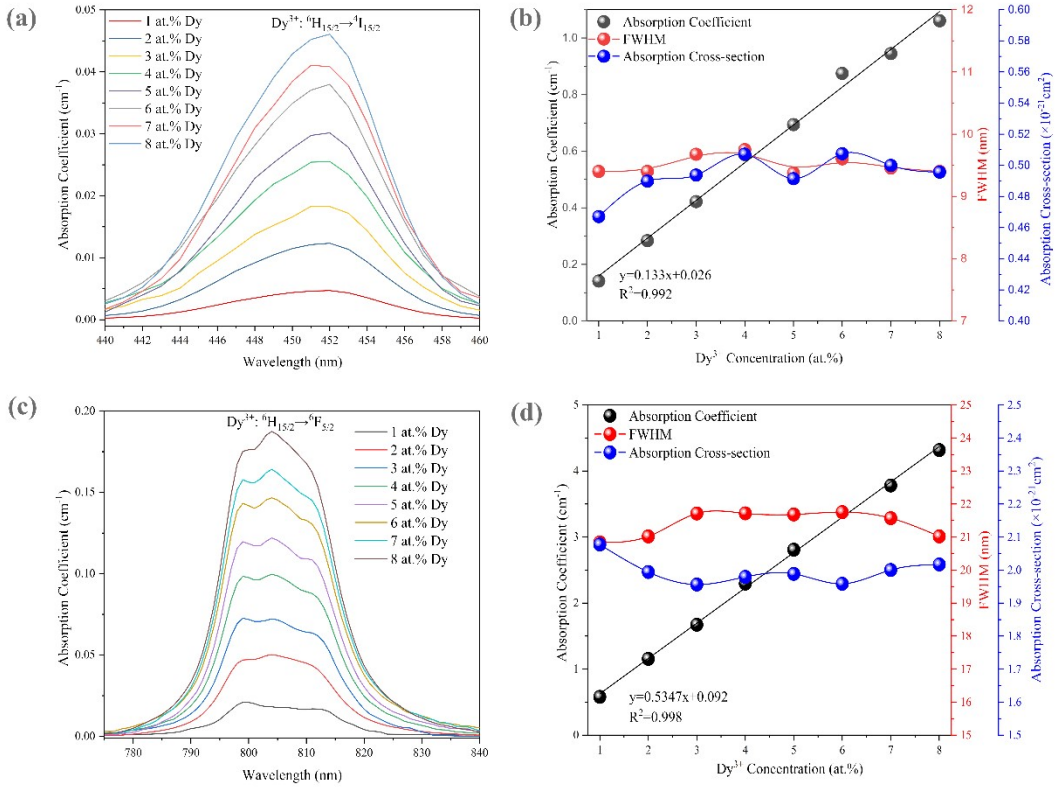

Figure S6. (a) Absorption characteristics corresponding to the Dy^{3+}: $^6H_{15/2}\rightarrow{}^4I_{15/2}$ transition at 452 nm for grown Dy^{3+}: CaF_2 crystals; (b) Absorption cross–section, absorption coefficient, and full width at half maximum at 452 nm for grown Dy^{3+}: CaF_2 crystals; (c) Absorption characteristics corresponding to the Dy^{3+}: $^6H_{15/2}\rightarrow{}^6F_{5/2}$ transition at 806 nm for grown Dy^{3+}: CaF_2 crystals; (d) Absorption cross–section, absorption coefficient, and full width at half maximum at 806 nm for grown Dy^{3+}: CaF_2 crystals.

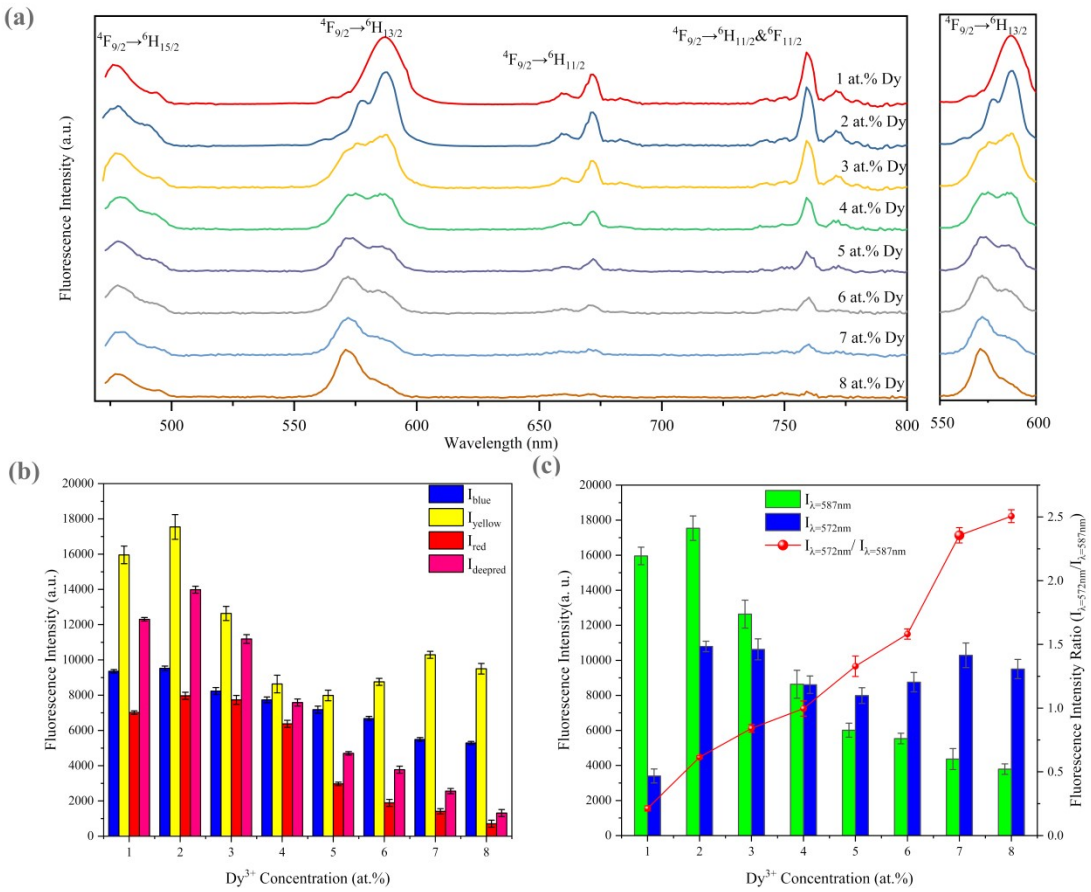

Figure S7. (a) Visible emission spectra in the 480–800 nm range of Dy^{3+}: CaF_2 crystals with different doping concentrations under 452 nm excitation; (b) Emission intensity variations of blue, yellow, red, and deep–red light with doping concentration; (c) Intensity variations and ratio of 587 nm and 572 nm yellow emissions with doping concentration.

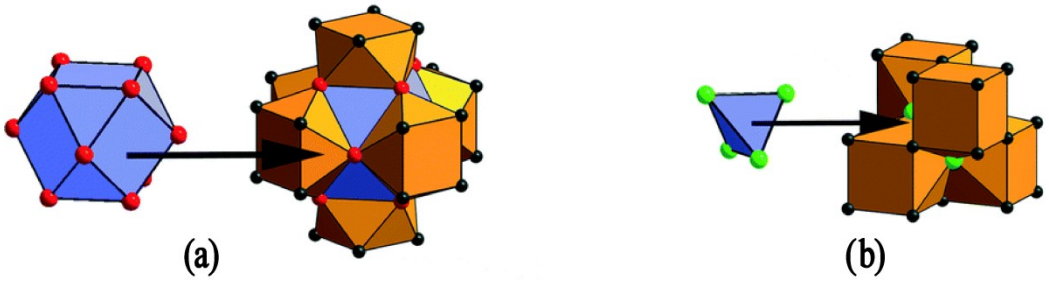

Figure S8. Schematic diagram of cluster structures: (a) M and N-type clusters, (b) L-type clusters.

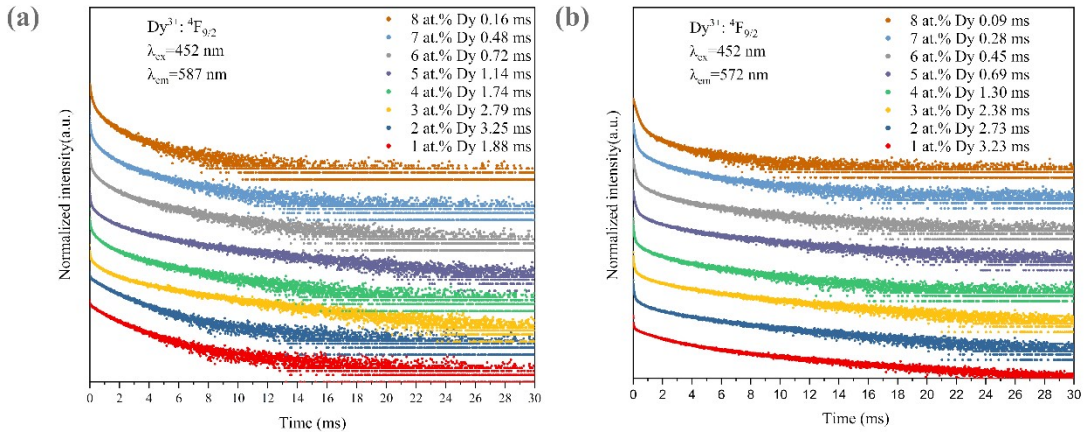

Figure S9. (a) Fluorescence decay curves monitored at 587 nm under 452 nm excitation; (b) Fluorescence decay curves monitored at 572 nm under 452 nm excitation.

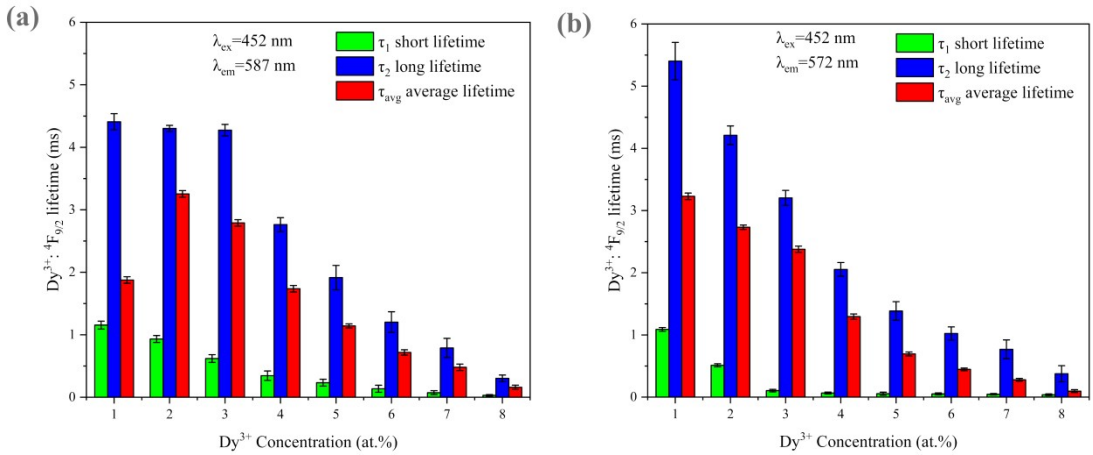

Figure S10. Concentration dependence of fluorescence lifetimes (short lifetime τ_1, long lifetime τ_2, and average lifetime τavg) of the $^4F_{9/2}$ level obtained from fitting the decay curves under 452 nm excitation, monitored at (a) 587 nm and (b) 572 nm.

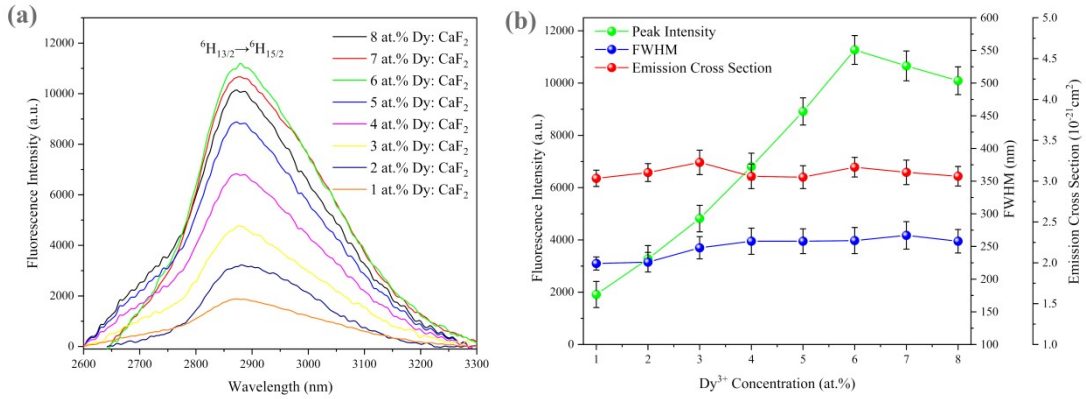

Figure S11. (a) MIR fluorescence spectra in the 2600–3300 nm band of Dy^{3+}: CaF_2 crystals with different doping concentrations under 806 nm excitation; (b) Variation of emission peak intensity, FWHM, and σ_{em} with doping concentration.

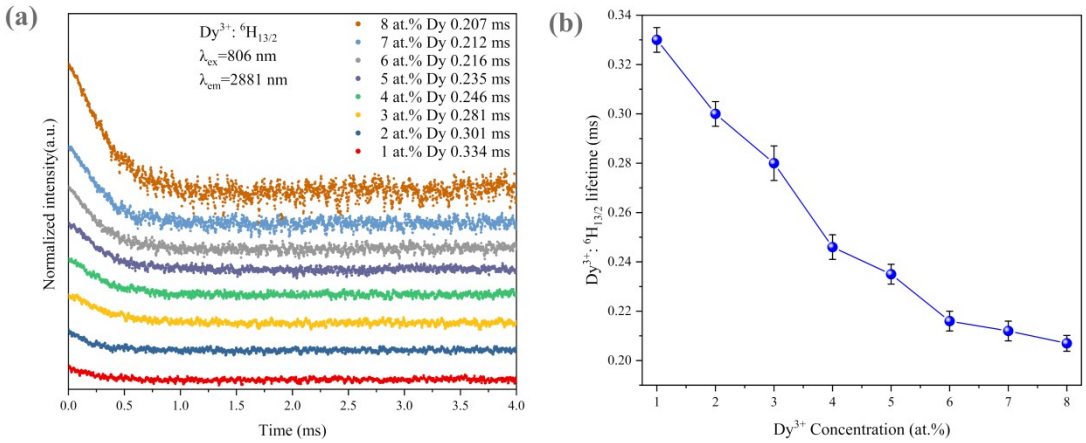

Figure S12. (a) Fluorescence decay curves monitored at 2881 nm under 806 nm excitation; (b) Lifetime variation of Dy^{3+}: $^6H_{13/2}$ level with doping concentration.